Analysis of ATP Binding to CheA Containing Tryptophan Substitutions near the Active Site†

Richard C. Stewart*

Department of Cell Biology & Molecular Genetics, University of Maryland, College Park, Maryland 20742

Received November 12, 2004; Revised Manuscript Received January 13, 2005

ABSTRACT: Signal transduction in the chemotaxis system of *Escherichia coli* involves an autophosphorylating protein histidine kinase, CheA. At the active site of CheA, phenylalanine residues 455 and 459 occupy positions near the ATP-binding pocket, immediately adjacent to one of the hinge regions of a loop that undergoes an ATP-induced conformational change ("lid closure") that has been characterized previously in X-ray crystal structures [Bilwes et al. (2001) *Nat. Struct. Biol. 8*, 353−360]. We generated versions of CheA carrying F455W and F459W replacements and investigated whether the fluorescence properties of the introduced tryptophan side chains were affected by nucleotide binding in a manner that would provide a signal for investigating the dynamics of active site events, such as ATP binding and lid closure. Our results indicate that CheA^{F455W} is useful in this regard, but CheA^{F459W} is not. CheA^{F455W} retained full catalytic activity and exhibited easily monitored fluorescence changes upon binding nucleotide: we observed a 25−30% decrease in CheA^{F455W} fluorescence emission intensity at 330 nm upon binding ATP in the absence of Mg^{2+}; in the presence of Mg^{2+}, the emission spectrum of the CheA^{F455W}:ATP complex was red-shifted by 5 nm and exhibited an increased intensity (∼20% higher at 345 nm relative to that of uncomplexed CheA^{F455W}). Different fluorescence changes were observed when two ATP analogues (ADPNP and ADPCP) were used instead of ATP and when Mn^{2+} or Ca^{2+} was used in place of Mg^{2+}. We exploited the fluorescence changes induced by Mg^{2+}−ATP to explore the kinetics and mechanism of nucleotide binding by CheA^{F455W}. In the absence of Mg^{2+}, binding appears to involve a simple one-step equilibrium (k_{assn} = 0.7 μM^{-1} s^{-1} and k_{dissn} = 270 s^{-1} at 4 °C). In the presence of Mg^{2+}, the binding mechanism involves at least two steps: (i) rapid, relatively weak binding followed by (ii) a rapid, reversible step ($k_{forward}$ = 300 s^{-1} and $k_{reverse}$ =15 s^{-1} at 4 °C) that enhanced the overall affinity of the complex and generated an increase in W455 fluorescence. This second step could reflect a conformational change at the CheA active site, such as lid closure. These results provide the first insight into the dynamics of nucleotide binding and substrate-induced conformational changes at the active site of a protein histidine kinase.

CheA[1] is an autophosphorylating protein histidine kinase (*1*, *2*); it functions in the signal transduction pathway that allows *Escherichia coli* and numerous other bacteria to accomplish chemotaxis, an ability that reflects control of cell swimming patterns in response to gradients of chemicals (attractants and repellents) encountered in the environment (*3*−*5*). The chemotaxis signal transduction pathway includes the following sequence of events: cell-surface receptor proteins detect prevailing extracellular concentrations of attractant/repellent and regulate the activity of CheA accordingly, CheA then regulates the activity of CheY, and CheY, in turn, interacts with the flagellar motors to modulate the direction of flagellar rotation in a manner that determines whether a cell will either continue swimming in its current direction or somersault to change direction (*6*−*8*).

Propagation of a signal from the receptors to the flagellar motors involves a series of phosphorylation and dephosphorylation reactions, the first of which is autophosphorylation by CheA (*9*). CheA acquires the γ-phosphoryl group of Mg^{2+}−ATP, covalently linking it to a specific histidine side chain (H48) (*1*, *2*). The rate of this autophosphorylation reaction is subject to regulation by the chemotaxis receptor proteins (*6*, *7*), slowing when receptors bind attractant molecules (such as various sugars and amino acids) and speeding up when these attractants dissociate or in the presence of repellent molecules. Autophosphorylated CheA can donate its phosphoryl group to either of two downstream signaling proteins, CheY or CheB (*1*, *10*), and these response regulator proteins become activated as a result of this phospho transfer. Phospho-CheY binds to the switch components of the flagellar motors in a manner that promotes clockwise rotation, thereby causing changes in the swimming direction (*11*, *12*). Phospho-CheB modifies the signaling properties of the chemotaxis receptor proteins in ways that promote sensory adaptation (*13*, *14*). The lifetimes of the activated (phosphorylated) forms of CheY and CheB are

† Supported by NIH Research Grant GM52853 to R.C.S.

* Phone: (301) 405-5475. Fax: (301) 314-9489. E-mail: rs224@umail.umd.edu.

[1] Abbreviations: ADPCP, β,γ-methyleneadenosine 5′-triphosphate; ADPNP, 5′-adenylylimidodiphosphate; P-CheA, phosphorylated CheA; PHK, protein histidine kinase; TNP-ATP, 2′(3′)-*O*-(2,4,6-trinitrophenyl)adenosine 5′-triphosphate; IPTG, isopropyl β-D-thiogalactoside.

10.1021/bi0476026 CCC: $30.25
Published on Web 02/22/2005

limited by their intrinsic autophosphatase activities and, for CheY, by a phosphatase, CheZ (*2*, *10*, *15*).

There are many signal transduction pathways that utilize proteins that are evolutionarily related to CheA, CheY, and CheB (*16*, *17*). For example, a single *E. coli* cell contains 62 distinct protein histidine kinases, each operating in a distinct sensory response pathway and each utilizing a distinct cognate response regulator (*18*). Hundreds of additional protein histidine kinases have been identified (by sequence comparisons) in prokaryotic genomes (*19*, *20*). In addition, PHKs appear to be present in some, but not all, eukaryotic microorganisms as well as in some plants (*21*). CheA is arguably the most intensively studied PHK: mutagenesis studies (*22*, *23*), biochemical investigations (*22*, *24*−*28*), and detailed structural information derived from NMR studies (*29*, *30*) and X-ray crystallography (*31*, *32*) have combined to provide some insight into the catalytic mechanism of CheA. A few other PHKs (*33*−*35*) have been examined in detail, providing support for the idea that these kinases make use of some common structural and mechanistic features. However, current understanding of the catalytic mechanism of this important class of protein kinases is not extensive or detailed. In particular, little information is available regarding ATP-induced conformational changes in PHKs. It seems likely that such changes must play an important role in the autophosphorylation reaction, as the phospho-accepting histidine side chain is located in a protein domain distinct from the domain containing the ATP-binding site (*36*).

The modular organization of CheA is depicted in Figure 1A. The active site of CheA includes an ATP-binding cavity (located in domain P4) and a flexible loop region (the "ATP lid") that appears to fold over the bound nucleotide in a manner similar to that observed for the GHL family of ATPases (Figure 1B) (*32*). Several of these ATPases appear to utilize this loop movement (lid closure) as an important part of their catalytic mechanism; it promotes shifts in the relative positions of domains within the protein, shifts that are required for these enzymes to act upon their substrates (*37*−*39*). Thus, it seems reasonable to propose that the lid closure in CheA could play a similar role, perhaps promoting the interdomain interactions required to bring the P1 domain (and H48) to the active site located in the P4 domain (*32*, *40*, *41*).

The CheA crystal structures defined by Bilwes et al. (*31*, *32*) have provided informative snapshots of different potential conformational states of the CheA active site: an open conformation in the absence of bound nucleotide, a partially closed conformation when Mg^{2+}-complexed nucleotide is bound, and an alternative, more compact active site observed in some CheA:nucleotide complexes lacking a divalent metal ion. To complement these static views of the nucleotide complex, it is important to investigate the dynamics of the CheA active site, such as the kinetics of interconversion between different conformations. Such information could be valuable for understanding the autophosphorylation mechanism of CheA and other PHKs. For example, purified CheA autophosphorylates slowly ($k_{cat} \approx 0.05\ s^{-1}$). Could this slowness reflect slow conformational changes at the active site? To begin addressing such questions, we introduced tryptophan substitutions at two selected positions near the CheA active site and then attempted to use these as fluorescent reporters of events at the active site. Our results with $CheA^{F455W}$ provide some insight into the mechanism of ATP binding and the kinetics of an active site conformational change resulting from this binding.

EXPERIMENTAL PROCEDURES

Materials. High-purity ATP and ADP were purchased from Roche Diagnostics Corp. (Indianapolis, IN). TNP-ATP was from Molecular Probes (Eugene, OR). DTT and IPTG were purchased from BioVectra (PEI, Canada). $MgCl_2$, $MnCl_2$, $CaCl_2$, ADPNP, ADPCP, Tris, glycerol, and Na_2EDTA were purchased from Sigma. TNKGDG buffer contained 50 mM Tris−HCl, 50 mM potassium glutamate, 25 mM NaCl, 0.5 mM DTT, and 10% glycerol (v/v) adjusted to pH 7.5 at 25 °C.

Site-Directed Mutants, Plasmids, and Bacterial Strains. Tryptophan substitution mutations were introduced into *cheA* using appropriate custom-synthesized oligonucleotides (Invitrogen) and the GeneTailor site-directed mutagenesis kit (Invitrogen). Mutations created unique silent restriction sites and were confirmed by DNA sequencing (University of Maryland Center for Agricultural Biotechnology).

E. coli K-12 derivatives RP3098 [Δ(*flhA*−*flhD*)] (*42*) and Δ*cheA* strain RP9535 (*43*) were kindly provided by Sandy Parkinson (University of Utah, Salt Lake City, UT). RP3098 has a chromosomal deletion that removes all of the *che* genes; this strain was used for plasmid-directed overproduction of $(His)_6$−$CheA^{wt}$ and $(His)_6$−$CheA^{H48Q}$ and each of the tryptophan-substitution versions of $(His)_6$−CheA and $(His)_6$−$CheA^{H48Q}$. Wild-type and mutant *cheA* alleles were expressed as N-terminal $(His)_6$ fusions using a derivative of plasmid pAR1:*cheA* (*23*).

To examine the ability of each CheA derivative to support chemotaxis, the corresponding *cheA* alleles (in plasmid pAR1) were transformed into Δ*cheA* host RP9535. Transformants were stabbed into trpytone swarm plates (*44*), and movement of the outer edges of the swarm colonies was measured (*45*) and compared to that observed for RP9535 carrying pAR1:$cheA^{wt}$ and pAR1 lacking *cheA*.

Protein Purification. Each of the versions of CheA used for this work carried an N-terminal $(His)_6$ tag to facilitate purification. To simplify the nomenclature in the text, hereafter we have omitted explicit inclusion of $(His)_6$ in the name of each protein. Previously published methods were used to purify these CheA derivatives (*23*) and CheY (*46*, *47*). Protein concentrations were determined using calculated extinction coefficients (*48*): 16.3 $mM^{-1}\ cm^{-1}$ for $CheA^{wt}$, 22.0 $mM^{-1}\ cm^{-1}$ for $CheA^{F455W}$ and $CheA^{F459W}$, 27.7 $mM^{-1}\ cm^{-1}$ for $CheA^{F455W,F459W}$, 8.25 $mM^{-1}\ cm^{-1}$ for CheY.

CheA Autokinase Assays. CheA autophorphorylation activity was assayed in two independent ways. The two different assays gave comparable results. In the first assay, CheA turnover was monitored spectrophotometrically using a coupling system to link ADP production to NADH oxidation, as described previously (*8*, *49*). These assays were performed at 25° C using TNKGDG buffer containing 5 mM $MgCl_2$ and 50 μM CheY. At this CheY concentration, CheA autophosphorylation is rate-limiting. The second autokinase assay monitored covalent attachment of ^{32}P to CheA in mixtures of CheA and [γ-^{32}P]ATP. SDS−PAGE analysis, quantitation of ^{32}P, and analysis of reaction time courses were performed as described previously (*24*, *50*).

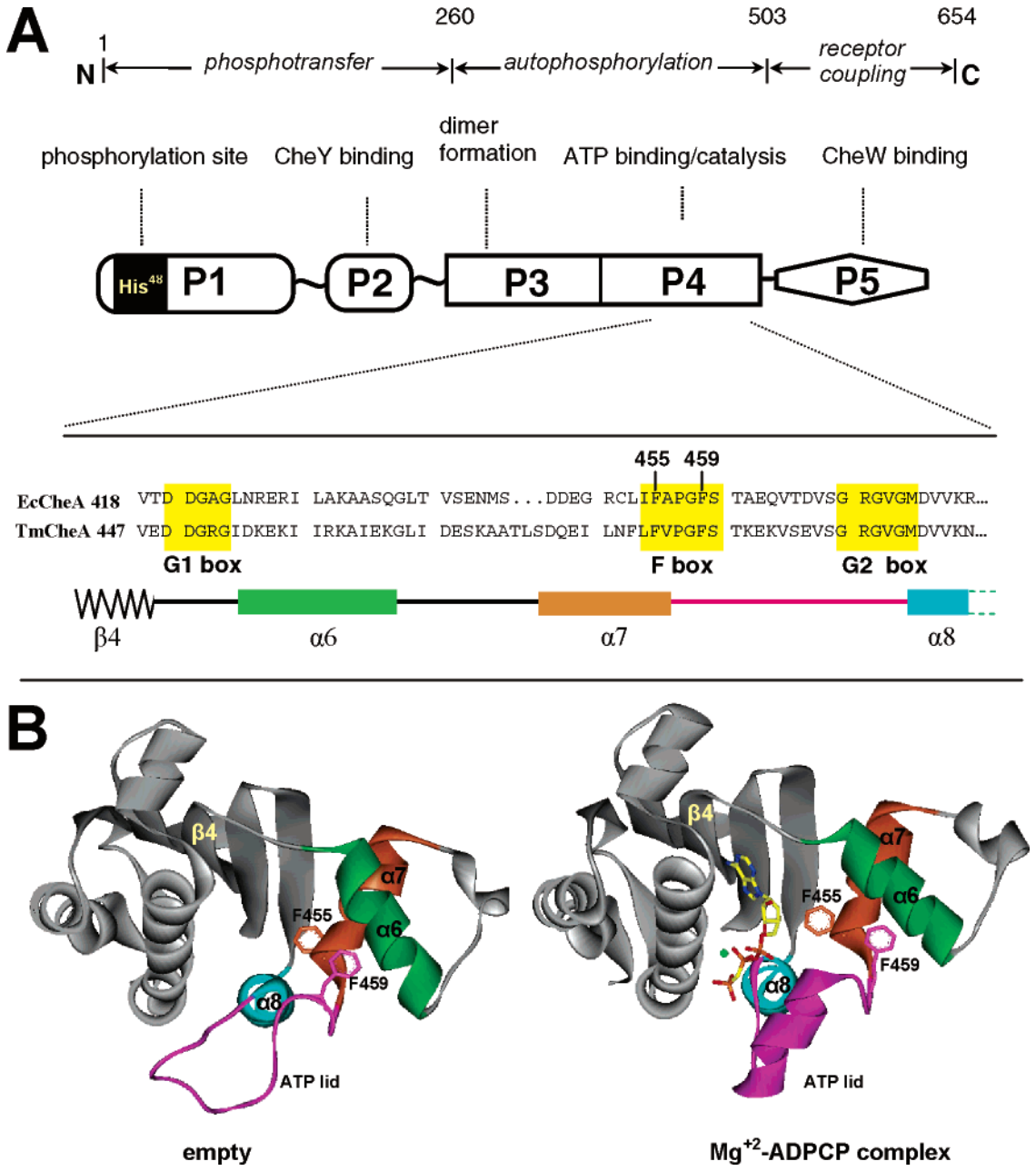

FIGURE 1: Schematic diagram of the functional organization of CheA (A) and structure of the ATP-binding site (B). (A) Domains P1−P5 of CheA have been defined by a variety of high-resolution methods, including NMR (*29*, *30*, *56*, *57*) and X-ray crystallography (*31*, *58*, *59*), and lower resolution approaches such as protease sensitivity (*60*). Functions have been assigned to these domains on the basis of information gleaned from biochemical and molecular genetic approaches (*2*, *26*, *60*, *61*). Domain P4 encompasses the ATP-binding site and active site of CheA (*32*). P4 includes four blocks of amino acids which are conserved sequence elements in the PHK superfamily (*16*, *19*). The amino acid sequences of three of these blocks (G1, F, and G2) are shown (highlighted in yellow) for *E. coli* CheA and *T. maritima* CheA. The locations of defined structural elements of P4 (α6 → α7) relative to G1, F, and G2 are depicted schematically below the sequences. The numbering of these helices corresponds to that used by Bilwes et al. (*31*) in their description of the crystal structure of a *T. maritima* fragment corresponding to domains P3−P5. (B) Effect of nucleotide binding on the conformation of the CheA active site. The structure on the left depicts the active site structure of *T. maritima* CheA in the absence of nucleotide (generated using coordinates from PDB file 1B3Q) (*31*). The structure on the right depicts the active site of *T. maritima* CheA with Mg^{2+}−ADPCP bound (PDB file 1I58) (*32*). The color-coding in these structures matches that used in panel A. Comparison of the empty active site to the Mg^{2+}−ADPCP-bound active site indicates that the ATP lid region (magenta) undergoes a conformational change upon nucleotide binding. The positions of the F box phenylalanine side chains relative to the ATP lid and bound nucleotide are shown. The indicated amino acid numbering (F455 and F459) corresponds to *E. coli* CheA, which we assume adopts an active site structure very similar to that of *T. maritima* CheA.

Fluorescence-Monitored Binding Titrations. Fluorescence emission and excitation spectra were recorded using a PTI QuantaMaster instrument. Samples in TNKGDG buffer (2.5 mL) were placed in quartz cuvettes (1 cm × 1 cm), stirred continuously using a magnetic stir bar, and maintained at constant temperature using a circulating water bath connected to the cuvette holder. CheA fluorescence was monitored by recording emission spectra (305−455 nm, slits at 5 nm) when the excitation wavelength was set at 296 nm (slits at 1.5 nm). This excitation wavelength was chosen to eliminate the effects of high ATP concentrations on the intensity of the excitation energy. In a typical experiment, successive additions of concentrated ATP (10 or 100 mM) were made to a solution containing 2.5 μM CheA, and emission spectra were

recorded following each addition. The samples were shielded from the excitation light between additions and did not appear to experience photobleaching (as indicated by the stability of the emission signal in "mock titrations" in which buffer was added in place of ATP). Results from ATP titrations were corrected for small dilution effects and then analyzed using least-squares fitting routines in Dynafit (*51*) or SigmaPlot. This analysis assumed a simple, one-site binding model. As CheA is a dimer under our experimental conditions (*28*), this assumption equates to assuming that the two nucleotide-binding sites of the dimer are identical and operate independently.

Rapid Reaction Measurements. Stopped-flow fluorescence experiments were performed using an Applied Photophysics SX-17MV instrument modified with a 2 μL observation cell that reduced the deadtime to ~0.8 ms (measured using the Massey procedure (*52*)). The excitation wavelength was set at 295 nm, and the emitted light (at >320 nm) was monitored by a photomultiplier after passing through a WG320 long-pass filter. Data collection and analysis were performed using the Applied Photophysics software. In a typical experiment, 10 consecutive stopped-flow shots were collected for each set of reaction conditions (e.g., at each ATP concentration) and then averaged prior to analysis to define the observed pseudo-first-order rate constant defined by the time course. The reactants were maintained at constant temperature using a circulating water bath.

RESULTS

Activities of CheA^{F455W} and CheA^{F459W} in Vitro and in Vivo. We used oligonucleotide-directed mutagenesis to generate *cheA* alleles encoding CheA^{F455W}, CheA^{F459W}, and CheA^{F455W,F459W}. We also generated variants of these proteins that carried, in addition, an H48Q substitution that rendered the proteins incapable of autophorphorylation (by removing the phosphorylation site). After purifying the $(His)_6$-tagged versions of these proteins as well as $(His)_6$-tagged CheA^{wt}, we assayed their autokinase activities as detailed in the Experimental Procedures. CheA^{F455W} exhibited a k_{cat} that is comparable to that of wild-type CheA and a somewhat lower K_m^{ATP} (Figure 2). CheA^{F459W} and CheA^{F455W,F459W} exhibited k_{cat} values (0.0006−0.001 s^{-1}) that are 1−2% of the wild-type value (results not shown). As expected, the H48Q versions of each of these proteins exhibited undetectable autokinase activities. These results indicate that CheA^{F455W} retains normal catalytic activity in vitro, while the F459W mutant and the F455W,F459W double mutant had greatly reduced autokinase activity.

To assess the ability of the different versions of CheA to function in an in vivo context, we used swarm plate assays (*44*) to observe the ability of each CheA variant to support chemotaxis when expressed at appropriate levels in a Δ*cheA* strain of *E. coli* (RP9535). We found that CheA^{F455W} supported a chemotactic swarming rate that was essentially the same as that observed when wild-type CheA was expressed in this strain (results not shown). These results suggest that, in vivo, the autokinase activity of CheA^{F455W} is regulated by the chemotaxis receptor proteins in a manner that is adequate to enable regulation of swimming movements in response to gradients of chemostimuli. None of the other CheA variants (CheA^{F459W}, CheA^{F455W,F459W}, CheA^{H48Q}, CheA^{H48Q,F455W}, and CheA^{H48Q,F459W}) enabled strain RP9535 to exhibit any observable chemotaxis ability in swarm assays: the swarm-plate colonies were indistinguishable from that observed for the host strain alone or carrying a plasmid lacking *cheA* (results not shown). The lack of complementation by *cheA*^{F459W} and *cheA*^{F455W,F459W} confirms previous observations with *cheA*^{F459Y} and *cheA*^{F455Y,F459Y} (*22*, *53*) and suggests that the very low autokinase activities of these versions of CheA are inadequate to support chemotaxis.

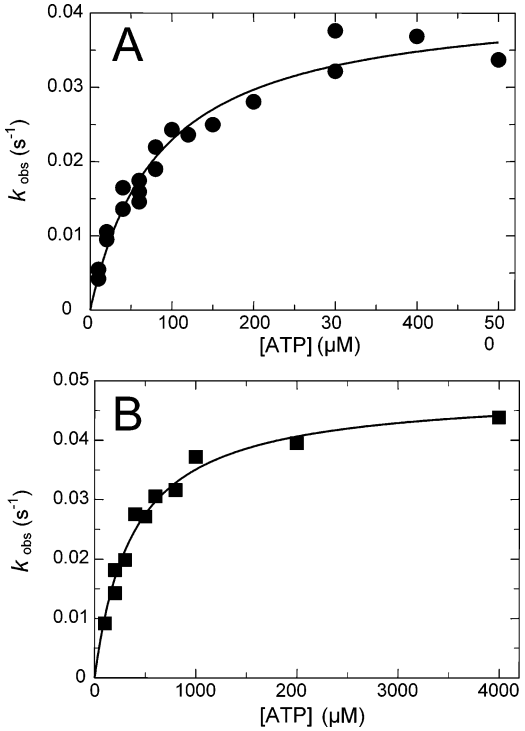

FIGURE 2: Steady-state kinetic parameters for autokinase activity of CheA^{F455W} (A) and CheA^{wt} (B). Autophosphorylation rates were measured at a series of ATP concentrations for reaction mixtures containing 2 μM CheA and 50 μM CheY in TNKGDG buffer containing 10 mM $MgCl_2$ and a coupling system comprised of 1 mM sodium phosphoenolpyruvate, 0.2 mM NADH, 30 units mL^{-1} lactate dehydrogenase, and 20 units mL^{-1} pyruvate kinase (*49*). ATP consumption was monitored by following the decrease in absorbance at 340 nm (reflecting oxidation of NADH by the coupling system). The curves (solid lines) indicate the best fit of the data using the Michaelis−Menten equation and least-squares analysis in SigmaPlot: for CheA^{F455W} (A), the best fit indicated $K_m^{ATP} = 85 \pm 10$ μM and $k_{cat} = 0.042 \pm 0.005$ s^{-1}; for CheA^{wt} (B), the best fit indicated $K_m^{ATP} = 380 \pm 20$ μM and $k_{cat} = 0.048 \pm 0.005$ s^{-1}.

Effect of Nucleotides on Fluorescence of CheA Tryptophan-Substitution Mutants. We examined the effect of ATP and ADP on the intrinsic fluorescence emission properties of CheA^{wt}, CheA^{F455W}, CheA^{F459W}, and CheA^{F455W,F459W}. To eliminate possible effects of catalytic turnover of ATP by CheA, we also repeated these experiments using versions of these proteins carrying an H48Q substitution. Comparable results were obtained with the H48-replete and H48Q versions of each CheA variant. Addition of ATP or ADP had no effect on the steady-state fluorescence properties of CheA^{wt} (and CheA^{H48Q}) in either the presence or absence of Mg^{2+} (results not shown). Similarly, the emission properties of CheA^{F459W} (and CheA^{H48Q,F459W}) were insensitive to nucleotide addition. However, ATP and ADP affected the fluorescence emission spectrum of CheA^{F455W} (and CheA^{H48Q,F455W}). The changes observed in the absence of

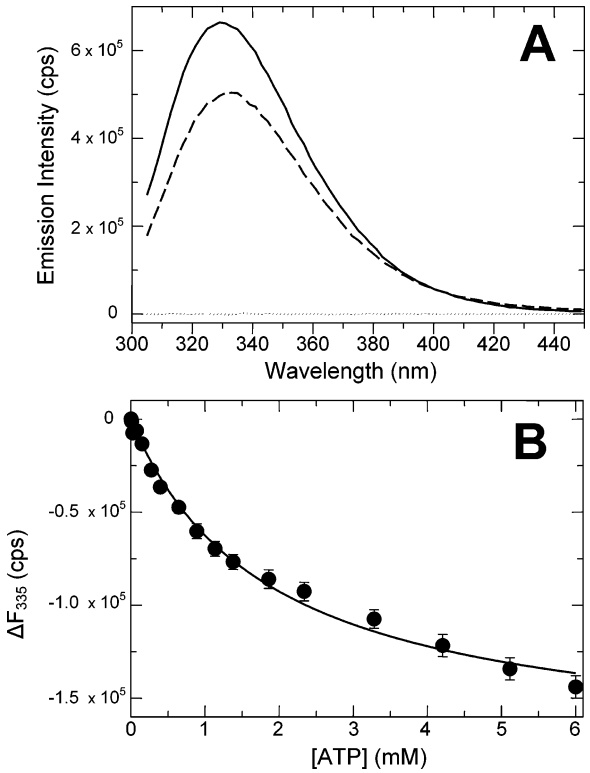

FIGURE 3: Effect of ATP on the fluorescence emission spectrum of CheA^{F455W} in the absence of Mg^{2+}. Spectra were recorded for CheA^{F455W} samples at 25 °C using λ_{ex} = 296 nm. (A) CheA^{H48Q,F455W} (2.5 μM) in the absence (—) or presence (---) of 10 mM ATP. Buffer was TNKGDG plus 10 mM Na_2EDTA. (B) Results of fluorescence-monitored titration of CheA^{H48Q,F455W} with ATP. The change in emission intensity at 335 nm (*y*-axis) was determined after each of a series of ATP additions to a 2.5 μM solution of CheA^{H48Q,F455W} in TNKGDG buffer containing 10 mM Na_2EDTA. The solid line shows the computer-generated best fit of the data using a simple, one-site binding equation (indicated $K_d = 1.8 \pm 0.2$ mM). Error bars indicate the standard error of the mean for each data point from two independent experiments.

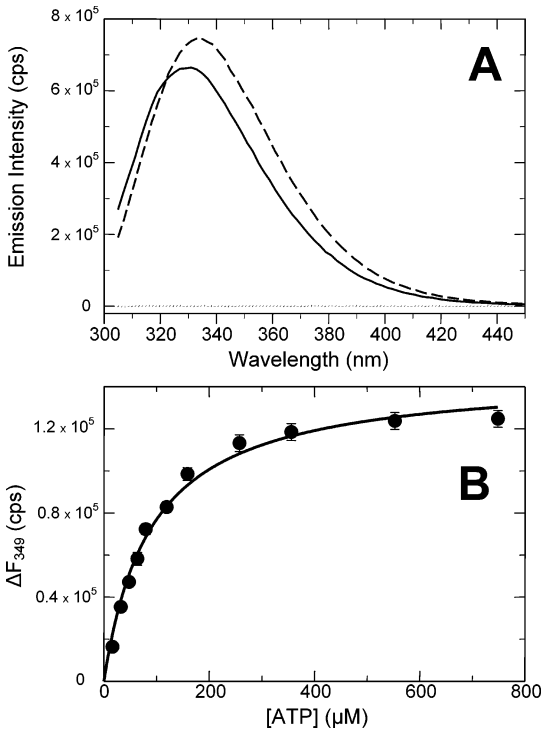

FIGURE 4: Effect of ATP on the fluorescence emission spectrum of CheA^{H48Q,F455W} in the presence of Mg^{2+}. Spectra were recorded for CheA^{H48Q,F455W} samples at 25 °C using λ_{ex} of 296 nm. (A) CheA^{H48Q,F455W} (2.5 μM) in the absence (—) or presence (---) of 10 mM ATP in TNKGDG buffer containing 10 mM $MgCl_2$. (B) Results of fluorescence-monitored titration of CheA^{H48Q,F455W} with ATP. The change in emission intensity at 349 nm (*y*-axis) was determined after each of a series of ATP additions to a 2.5 μM solution of CheA^{H48Q,F455W} in TNKGDG buffer containing 10 mM $MgCl_2$. The solid line shows the computer-generated best fit of the data using a simple, one-site binding equation (indicated $K_d = 90 \pm 10$ μM). Error bars indicate the standard error of the mean for each data point from three independent experiments.

Mg^{2+} were different from those observed in its presence (Figures 3 and 4). In the absence of Mg^{2+}, addition of a saturating level of ATP resulted in a significant decrease (25−30% at 330 nm) in emission intensity for CheA^{F455W} (Figure 3A). A similar decrease was observed upon addition of saturating ADP (results not shown). In the presence of Mg^{2+} (Figure 4A), addition of saturating levels of ATP (or ADP) resulted in a 5 nm red shift of the emission spectrum of the CheA^{F455W} (and CheA^{H48Q,F455W}) and an increased emission intensity (~20% higher at 345 nm relative to that of uncomplexed CheA^{F455W}). These changes (i.e., an increased emission intensity and red shift) were not observed with the double mutant CheA^{F455W,F459W} (and its H48Q version): with the FW double mutant, fluorescence emission intensity decreased upon addition of ATP or ADP in the presence or absence of Mg^{2+} to an extent similar to that shown in Figure 3A (results not shown).

We performed fluorescence-monitored titrations of CheA^{H48Q,F455W} with ATP. A plot of the extent of fluorescence decrease as a function of ATP concentration in the absence of Mg^{2+} (Figure 3B) indicated a hyperbolic relationship, as expected for a reversible binding equilibrium in which the CheA^{F455W}:ATP complex has lower emission intensity than the free CheA^{F455W}. Analysis of the titration profile (Figure 3B) indicated that the binding curve could be fit well using a simple one-site model with a K_d of ~1.8 mM for the CheA^{F455W}:ATP complex at 25 °C. The K_d value at 4 °C was ~400 μM (data not shown). For similar titrations in the presence of 10 mM Mg^{2+}, we monitored formation of the CheA^{F455W}:Mg^{2+}−ATP complex by following the increase in emission intensity at 350 nm (Figure 4B). Analysis of these binding curves indicated tighter binding than in the absence of Mg^{2+} (in the presence of 10 mM Mg^{2+}, K_d = 90 μM at 25 °C and 40 μM at 4 °C). Similar results were obtained using ADP instead of ATP, but the K_d values were somewhat lower (e.g., K_d = 12 μM at 4 °C for the CheA^{F455W}:Mg^{2+}−ADP complex). The K_d of the CheA^{F455W}:Mg^{2+}−ATP complex is lower than that determined previously (using different approaches) for the wild-type CheA:Mg^{2+}−ATP complex (K_d = 200−300 μM) (*23*, *54*). As discussed in the preceding section, we observed a similar difference in K_m^{ATP} values determined from steady-state assays of CheA autokinase activity (80 μM forCheA^{F455W} versus 380 μM for CheA^{wt}). These results indicate that CheA^{F455W} binds Mg^{2+}−ATP with higher affinity than does CheA^{wt}. Our findings also indicate that Mg^{2+} enhances the affinity of the active site of CheA^{F455W} for ATP in a manner similar to that reported previously for the wild-type active site (*54*).

Effects of ATP Analogues and Alternative Divalent Metal Ions on CheA^{F455W} Fluorescence. The X-ray crystallography

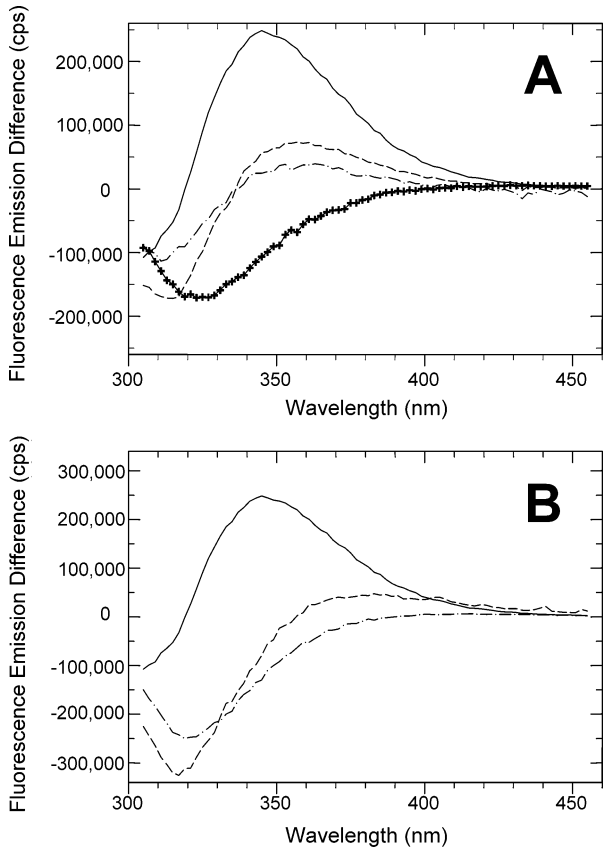

FIGURE 5: Effect of different nucleotides and alternative metal ions on the fluorescence emission spectrum of CheA^{H48Q,F455W}. (A) Difference spectra for 5 μM CheA^{H48Q,F455W} in the presence of saturating levels of Mg^{2+}−ATP (—), Mn^{2+}−ATP (---), and Ca^{2+}−ATP(-•-). Each difference spectrum represents the emission spectrum observed in the presence of 5 mM metal−nucleotide *minus* the emission spectrum for the same CheA^{H48Q,F455W} solution before addition of the nucleotide. For comparison, the ATP-induced difference spectrum in the absence of any divalent metal ion is shown (+++). (B) Difference spectra for CheA^{H48Q,F455W} complexes with Mg^{2+}−ATP, Mg^{2+}−ADPCP, and Mg^{2+}−ADPNP. Each difference spectrum represents the emission spectrum observed in the presence of 5 mM metal−nucleotide *minus* the emission spectrum for the same CheA^{H48Q,F455W} sample before addition of the nucleotide.

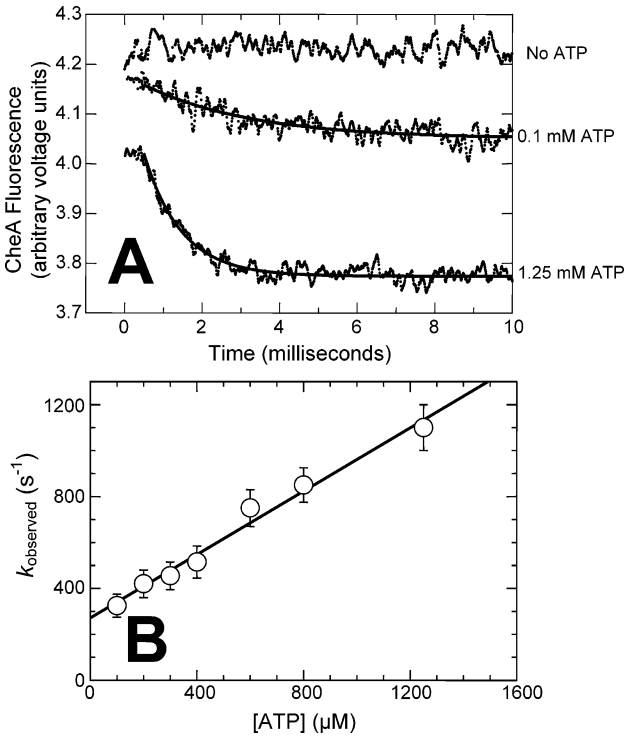

FIGURE 6: Kinetics of ATP binding to CheA^{H48Q,F455W} in the absence of Mg^{2+}. (A) Fluorescence stopped-flow measurements of emission intensity (λ_{ex} = 295 nm, λ_{em} > 320 nm) were made after 50 μL of a 10 μM CheA^{H48Q,F455W} sample was mixed with an equal volume of ATP at 4 °C in TNKGDG buffer containing 10 mM Na_2EDTA. Analysis of each time course as a single-exponential decay indicated $k_{observed}$ values (e.g., 325 s^{-1} at 100 μM ATP and 1050 s^{-1} at 1.25 mM ATP). The solid lines depict the computer-generated best fits that defined these $k_{observed}$ values. The "No ATP" time course was recorded using the same detector settings (PMT voltage and offset) as the 100 μM ATP and 1.25 mM ATP time courses and indicates that we were able to observe ~65% of the time course at the lowest ATP level (35% occurred during the instrument deadtime) and ~55% of the time course at the highest ATP level (45% occurred during the instrument deadtime). (B) Analysis of the effect of ATP concentration on the rate of complex formation. The plot of $k_{observed}$ versus ATP concentration is fit well by a line having a slope of 0.7 μM^{-1} s^{-1} and a *y*-axis intercept of 270 s^{-1} (both values defined by least-squares fitting). Error bars indicate the standard of the mean for data points representing averages of two independent experiments.

studies of Bilwes et al. (*32*) demonstrated that the active site of CheA undergoes a conformational change upon binding nucleotides and that slightly different conformations (especially of the loop region comprising the ATP lid) are generated depending on (i) the identity of the nucleotide bound and (ii) the nature of the divalent metal coordinated to the polyphosphate region of the nucleotide (Mn^{2+} versus Mg^{2+}). For example, subtly different active site conformations are induced by ADP, ADPNP, and ADPCP, and the Mg^{2+}−nucleotide-bound active site differs from that observed with the Mn^{2+}−nucleotide complex. We investigated the effects of alternative divalent metals (Mn^{2+} and Ca^{2+}) and two nonhydrolyzable ATP analogues (ADPNP and ADPCP) on the fluorescence properties of CheA^{F455W}. Our results indicate that Mn^{2+}−ATP and Ca^{2+}−ATP induced less dramatic fluorescence changes in CheA^{F455W} than did Mg^{2+}−ATP (Figure 5A). All three divalent metals effectively enhanced the affinity of the protein for ATP (results not shown). Similarly, we observed that the fluorescence properties of the CheA^{F455W}:nucleotide complex were different when ADPCP and ADPNP were used in place of ATP (Figure 5B). These results indicate that the fluorescence emission properties of W455 respond to subtle alterations in the conformation of the CheA active site and its bound nucleotide.

Nucleotide-Binding Dynamics. We examined the kinetics of nucleotide binding and dissociation by exploiting the change in fluorescence caused by binding of ATP to CheA^{F455W}. Using a stopped-flow fluorescence instrument, we first monitored ATP binding to CheA^{H48Q,F455W} in the absence of Mg^{2+}. These experiments were performed at 4 °C because the reactions were too fast to observe at 25 °C (they were essentially complete within the instrument deadtime). Time courses obtained at a series of ATP concentrations could be fit well by a single-exponential equation that defined a pseudo-first-order rate constant ($k_{observed}$) for each reaction (Figure 6A). The dependence of $k_{observed}$ on ATP concentration exhibited a linear relationship with a nonzero *y*-axis intercept; there were no indications of saturation kinetics (Figure 6B). The simplest reaction scheme that can

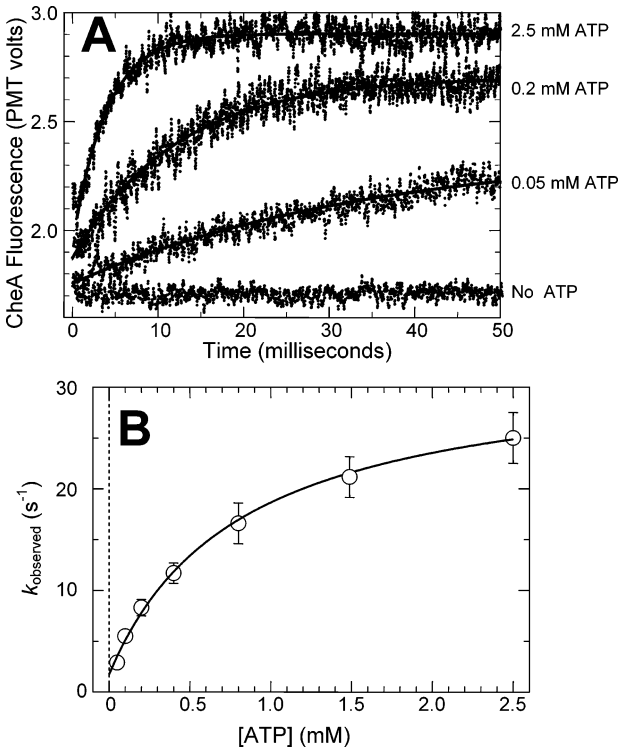

FIGURE 7: Kinetics of ATP binding to $CheA^{H48Q,F455W}$ in the presence of Mg^{2+}. (A) Fluorescence stopped-flow measurements of emission intensity (λ_{ex} = 295 nm, λ_{em} > 320 nm) were made after 50 μL of a 10 μM $CheA^{H48Q,F455W}$ sample was mixed with an equal volume of ATP at 4 °C in TNKGDG buffer containing 10 mM $MgCl_2$. Analysis of each time course as a single-exponential decay indicated $k_{observed}$ values (29 s^{-1} at 0.05 mM ATP, 85 s^{-1} at 0.2 mM ATP, 255 s^{-1} at 2.5 mM ATP). The solid lines depict the computer-generated best fits that defined these $k_{observed}$ values. The "No ATP" time course was recorded using the same detector settings (PMT voltage and offset) as the other time courses and indicates that we were able to observe 67% of the total fluorescence change at the highest ATP concentration (45% occurred in the deadtime) and 90−95% at the lowest ATP concentration. (B) Analysis of the effect of ATP concentration on the rate of complex formation. The plot of $k_{observed}$ versus ATP concentration indicates saturation kinetics and is fit well by a three-parameter hyperbola (solid line) defined by a maximal (extrapolated) $k_{observed}$ value of 306 s^{-1} at saturating ATP levels, a half-maximal $k_{observed}$ value at an ATP concentration of 810 μM, and a *y*-axis intercept of 17 s^{-1}.

account for these results is a simple, one-step reversible binding mechanism

$$\text{CheA} + \text{ATP} \underset{k_{-1}}{\overset{k_1}{\rightleftharpoons}} \text{CheA:ATP} \qquad (1)$$

for which $k_{observed} = k_{-1} + k_1[\text{ATP}]$. Our results indicate $k_1 = 0.7\ \mu M^{-1}\ s^{-1}$ and $k_{-1} = 270\ s^{-1}$. The ratio of these values (k_{-1}/k_1 = 385 μM) is close to the K_d value defined in the equilibrium titrations described above (400 μM at 4 °C). This agreement lends support to the idea that eq 1 adequately describes the binding equilibrium in the absence of Mg^{2+}.

Similar stopped-flow experiments were performed (also at 4 °C) to monitor ATP binding to $CheA^{H48Q,F455W}$ in the presence of Mg^{2+}. The time courses followed the increase in fluorescence emission and were fit well by a single-exponential equation (Figure 7A). The dependence of $k_{observed}$ on ATP concentration (Figure 7B) indicated saturation at high ATP levels and defined a hyperbolic dependence characterized by (i) an extrapolated maximal rate constant of 310 s^{-1} (below we refer to this as k_{max}), (ii) a $k_{observed}$ value equal to half of k_{max} at an ATP concentration of 800 μM (below we refer to this value as K_d^{kin}, the "kinetically defined K_d"), and (iii) a nonzero *y*-axis intercept (17 s^{-1}). These results are consistent with a two-step reaction mechanism

$$\text{CheA} + \text{Mg}^{2+}\text{−ATP} \underset{k_{-1}}{\overset{k_1}{\rightleftharpoons}} \text{CheA:Mg}^{2+}\text{−ATP} \underset{k_{-2}}{\overset{k_2}{\rightleftharpoons}} (\text{CheA:Mg}^{2+}\text{−ATP})^* \qquad (2)$$

in which the first $CheA:Mg^{2+}$−ATP complex is spectrally silent (i.e., has the same fluorescence as uncomplexed CheA) and the final complex has enhanced fluorescence emission. For such a reaction scheme, the relationships between the observable kinetic parameters extracted from Figure 7B (k_{max}, K_d^{kin}, *y*-axis intercept) and the rate constants for individual steps (k_1, k_{-1}, k_2, k_{-2}) will depend on the relative magnitudes of these rate constants, in particular the relative rates of k_{-1} and k_2 (*55*). These relationships are explored further in the Discussion.

For some combinations of *k* values (e.g., when $k_{-2} \ll k_{-1}$), the *y*-axis intercept of Figure 7B would indicate the value of k_{-2}, i.e., the rate constant for the rate-limiting step in dissociation of Mg^{2+}−ATP from the complex (*55*). To explore this possibility, we used an independent approach to monitor the kinetics of Mg^{2+}−ATP dissociation from $CheA^{F455W}$. In a stopped-flow fluorescence instrument, we rapidly mixed $CheA:Mg^{2+}$−ATP with excess TNP-ATP and monitored the ensuing increase in fluorescence at λ_{em} > 420 nm (λ_{ex} = 390 nm). This approach took advantage of the high-affinity binding of TNP-ATP to the CheA active site (K_d = 0.5 μM), the very rapid binding kinetics of this binding (Figure 8), and the resulting dramatic increase in TNP fluorescence that reflects its hydrophobic environment upon binding (*32*, *54*). These experiments (Figure 8A) indicated a rate constant of 15 s^{-1} for the overall dissociation of the $CheA^{F455W}:Mg^{2+}$−ATP complex at 4 °C (100 s^{-1} at 25 °C). This value corresponds well with that defined by the *y*-axis intercept of Figure 7B, supporting the idea that k_{-2} = 15 s^{-1}. A similar set of experiments (Figure 8B) using the wild-type $CheA:Mg^{2+}$−ATP complex (or $CheA^{H48Q}:Mg^{2+}$−ATP) defined a dissociation rate constant of 140 s^{-1} at 4 °C (460 s^{-1} at 25 °C), indicating that dissociation of Mg^{2+}−ATP from the $CheA^{F455W}$ active site is slower than from the wild-type active site. This difference is discussed below.

DISCUSSION

Amino acids F455 and F459 of the CheA reside in a short block of 5−8 amino acids, referred to as the "F box" (*16*), that is conserved in many, but not all, protein histidine kinases (*19*). In the 3-dimensional structure of CheA, the F box occupies a position immediately adjacent to the ATP-binding cavity. Crystal structures of CheA:nucleotide complexes indicate that side chains and backbone components of F box residues do not appear to interact directly with bound nucleotide, nor with the associated Mg^{2+}, but these residues are located immediately adjacent to the ATP lid, the flexible loop region that undergoes conformational changes when nucleotide binds to the active site (*32*). For example, in crystal structures of the P4 domain of *Thermo-*

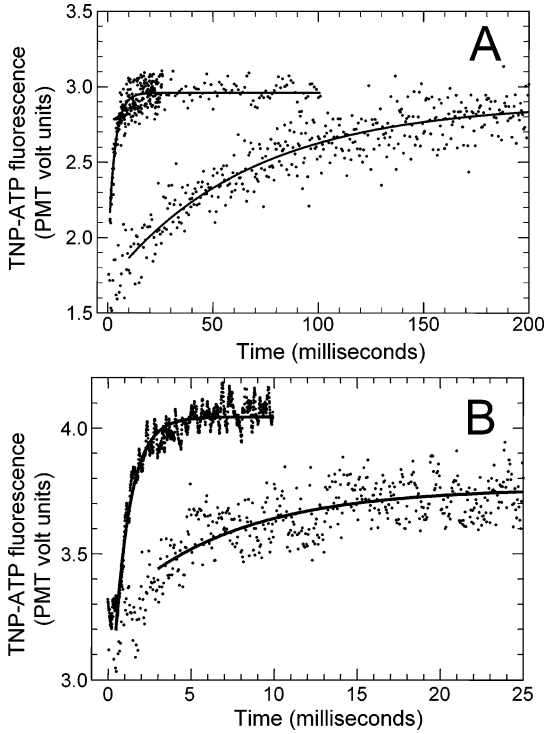

FIGURE 8: Kinetics of Mg^{2+}−ATP dissociation from $CheA^{H48Q,F455W}$ (A) and $CheA^{H48Q}$ (B). A stopped-flow instrument was used to monitor the fluorescence emission intensity of TNP-ATP (λ_{ex} = 390 nm, λ_{em} > 420 nm) immediately after rapid mixing of CheA samples with saturating concentrations (200 or 400 μM) in TNKGDG buffer containing 10 mM $MgCl_2$ at 4 °C. The observed fluorescence increase results from binding of the TNP-ATP to the CheA active site; previous work has demonstrated that this binding is competitive with ATP binding and has much higher affinity (K_d < 1 μM (*32*, *54*)). (A) Two time courses are shown: the more rapid time course shows that binding of 200 μM TNP-ATP to $CheA^{H48Q,F455W}$ (in the absence of any other nucleotide) is essentially complete within 10 ms ($k_{observed}$ = 330 s^{-1}); the slower time course ($k_{observed}$ = 15 s^{-1}) shows the binding reaction that occurs when 200 μM TNP-ATP is rapidly mixed with a preequilibrated solution containing 10 μM $CheA^{H48Q,F455W}$ and 100 μM ATP. The solid line in the faster time course shows the best fit of the entire time course using a single-exponential equation; the solid line in the slower time course shows the best fit obtained using a single-exponential equation and the data points *after* the first 10 ms. We interpreted the latter $k_{observed}$ value (which was >20-fold slower than that for TNP-ATP binding) as indicating the kinetics of Mg^{2+}−ATP dissociation from the active site of $CheA^{H48Q,F455W}$. (B) Two time courses are shown: the more rapid time course shows that binding of 400 μM TNP-ATP to $CheA^{H48Q}$ (in the absence of any other nucleotide) is essentially complete within 3 ms ($k_{observed}$ ≈ 1000 s^{-1}); the slower time course ($k_{observed}$ = 140 s^{-1}) shows the binding reaction that occurs when 400 μM TNP-ATP is rapidly mixed with a preequilibrated solution containing 10 μM $CheA^{H48Q}$ and 300 μM ATP. The solid line in the faster time course shows the best fit of the entire time course using a single-exponential equation; the solid line in the slower time course shows the best fit obtained using a single-exponential equation and the data points *after* the first 3 ms. We interpreted this slow $k_{observed}$ value as reflecting the kinetics of Mg^{2+}−ATP dissociation from the wild-type active site of $CheA^{H48Q}$.

toga maritima CheA, this loop is relatively unstructured and mobile, but when the protein binds Mg^{2+}−ADPCP, the loop assumes a more ordered, helical conformation that folds partway over the ATP-binding pocket as depicted in Figure 1. F455 is located at the end of helix 7 in P4 (Figure 1) immediately preceding the ATP lid, while F459 could be considered to be a part of the hinge region for the lid, or even a part of the lid itself.

Our results demonstrate that the side chain of F455 is not necessary for ATP binding or for catalysis of CheA autophosphorylation. The environment surrounding position 455, however, appears to be sensitive to active site events, such that an F455W substitution provides a sensitive fluorescent probe of ATP binding. This enabled our investigations of the kinetics of nucleotide binding and dissociation at the CheA active site. Before discussion of those aspects of our results, however, it is important to consider the nature of the events that give rise to the fluorescence increase caused by binding of Mg^{2+}−ATP to $CheA^{F455W}$. One intriguing possibility is that this increase results from the conformational change (lid closure) that accompanies Mg^{2+}−ATP binding to the CheA active site. The crystallography studies of Bilwes et al. (*32*) provide a structural context for considering this possibility. In particular, those studies allow us to make three relevant observations: (i) The conformation of the CheA active site is influenced by the divalent metal bound to the nucleotide. P4−nucleotide complexes that lacked a divalent metal exhibited less extensive lid closure and more compact binding cavities compared to their metal-replete counterparts. Also, Mg^{2+} enabled more extensive lid closure than did Mn^{2+}. (ii) The conformation of the lid region is affected by relatively subtle changes in the charge distribution and conformation of the polyphosphate groups of the bound nucleotide. For example, Mg^{2+}−ADPCP and Mg^{2+}−ADPNP caused different degrees of lid closure. (iii) Analysis of the protein−nucleotide-binding contacts suggests that lid closure is not required for nucleotide binding, but it is likely to be essential for catalytic activity. Thus, mutations affecting the conformation or flexibility of the lid region would be expected to hinder catalytic activity but not necessarily ATP binding.

Our fluorescence results provide the following parallels to this structural information: (i) When ATP binds to $CheA^{F455W}$, a fluorescence increase is observed only when a divalent metal ion is present, and in this regard Mg^{2+} was more effective than Mn^{2+}, which was more effective than Ca^{2+}. (ii) Binding of Mg^{2+}−ATP (Mg−ADP) to $CheA^{F455W}$ generated the largest fluorescence increase; Mg^{2+}−ADPCP and Mg^{2+}−ADPNP caused considerably smaller spectral changes. (iii) The F455W,F459W double mutant did not exhibit a fluorescence increase in the presence of Mg^{2+}−ATP, although it clearly bound the nucleotide as evidenced by quenching of the fluorescence emission. We speculate that an F−W substitution at position 459 might limit the ability of the hinge region spanning position 459 to effect lid closure. Such a mutant would be expected to be capable of binding ATP but would be ineffective as an autokinase, as we observed. Taken together, these observations support the hypothesis that the fluorescence emission of W455 responds to conformational changes of the ATP lid or to other closely related conformational changes at the CheA active site.

Our analysis of the nucleotide-binding kinetics suggests that ATP binding to CheA is a more complex process in the presence of Mg^{2+} than in its absence. Results obtained in the absence of a divalent metal are consistent with a simple, one-step binding equilibrium (eq 1). By contrast, in the presence of Mg^{2+}, the binding reaction exhibits saturation kinetics, suggesting that binding involves at least two reversible steps (eq 2). For such a reaction scheme, the effect

of ATP concentration on the overall kinetics would be defined by (*55*)

$$k_{\text{observed}} = \frac{k_1 k_2[\text{ATP}]}{(k_1[\text{ATP}] + k_{-1})} + k_{-2} \quad (3)$$

A plot of k_{observed} versus [ATP] would define a *y*-axis intercept of k_{-2}, a maximal k_{observed} value of $k_2 + k_{-2}$ at saturating ATP concentrations, and half-maximal k_{observed} at an ATP concentration equal to

$$K_{\text{d}}^{\text{kin}} = \frac{(k_{-1} + k_{-2})}{k_1 k_2} \quad (4)$$

It is informative to consider the possibility that the first step in this two-step binding mechanism (eq 2) is essentially the same as that observed in the absence of Mg^{2+} (eq 1) and that the second step of eq 2 involves a protein conformational change (such as closure of the ATP lid) that takes place only when Mg^{2+} is present. Given the values of k_1 (0.7 μM^{-1} s^{-1}) and k_{-1} (270 s^{-1}) defined for ATP binding in the absence of Mg^{2+}, and the value of k_2 (310 s^{-1}) defined by the maximal extrapolated k_{observed} value in Figure 7B, eq 4 would predict a $K_{\text{d}}^{\text{kin}}$ value of 828 μM, which corresponds quite well with the experimentally determined value of 810 μM (Figure 7B). This analysis supports the idea that ATP binding involves a rapid, low-affinity binding step (Mg^{2+}-independent) followed by a rate-limiting conformational change in the protein (requiring Mg^{2+}).

If the first step of Mg^{2+}−ATP binding to $CheA^{F455W}$ is indeed similar or identical to the one-step ATP-binding mechanism observed in the absence of Mg^{2+}, then one might expect to observe biphasic binding time courses for Mg^{2+}−ATP binding: a rapid fluorescence decrease (reflecting formation of a CheA:ATP complex) followed by an increase in fluorescence resulting from the Mg^{2+}-dependent conformation change. We did not observe biphasic time courses or any indications of a lag phase that might reflect composite effects of fluorescence decreases and increases. However, the low affinity of the first binding step and the similar rates of the first and second steps would make it difficult to detect such deviations from simple exponential behavior. In addition, it is possible that (unlike the Mg-free $CheA^{F455W}$:ATP complex) the first $CheA^{F455W}$:Mg^{2+}−ATP complex does not have diminished fluorescence: perhaps Mg^{2+} affects the ability of the ATP to alter the environment of W455 in the first step.

It seems reasonable to assume that ATP lid closure is a necessary step in the catalytic mechanism of CheA autophosphorylation (*31*, *32*). This conformational change might, for example, create an interaction surface for the domain (P1) containing the phosphorylation site, or it might trigger reorientation of other components of CheA. If we accept the more speculative premise that this lid closure is responsible for the fluorescence increase of $CheA^{F455W}$ observed when Mg^{2+}−ATP binds, then we can make some general statements about the nature of this conformational change. First, in such a scenario, our values of k_2 and k_{-2} would represent the rate constants for lid closure and opening, respectively. Both values are considerably higher than k_{cat} of the autophosphorylation reaction (~0.05 s^{-1}), leading to the conclusion that lid closure is not rate limiting for the autokinase reaction.

Interestingly, the K_{d} value for the $CheA^{F455W}$:Mg^{2+}−ATP complex is 4-fold lower than the corresponding value for wild-type CheA. This tighter binding of Mg^{2+}−ATP by $CheA^{F455W}$ raises an important question: how well does $CheA^{F455W}$ serve as a model for understanding the active site of wild-type CheA? It is conceivable, for example, that the two-step binding mechanism we observed with $CheA^{F455W}$ is not utilized by wild-type CheA. This possibility is difficult to test directly, but it seems unlikely when the following observations are considered together: (i) The k_{cat} value of $CheA^{F455W}$ is not much different from that of wild-type CheA, indicating that the active site of the mutant protein has not been altered significantly and that it likely binds Mg^{2+}−ATP in the same orientation as does the wild-type active site. (ii) The distance separating the adenine rings of ATP and the W455 side chain is likely to be >10 Å (assuming orientations similar to those reported by Bilwes et al. (*32*)), a separation that would preclude direct interactions of the tryptophan and adenine rings. (iii) The different K_{d} values observed for $CheA^{wt}$ and $CheA^{F455W}$ can be accounted for entirely by different values of k_{-2} for the respective CheA:Mg^{2+}−ATP complexes. Specifically, k_{-2} for $CheA^{F455W}$:Mg^{2+}−ATP is 100 s^{-1} at 25 °C, while the value measured for the wild-type CheA complex is 460 s^{-1}. This difference in k_{-2} (a ratio of 4.6) would result in a corresponding 4.6-fold difference in K_{d} ($k_{-2}k_{-1}/k_1k_2$) if the other steps of the binding/dissociation reactions (defined by k_1, k_{-1}, and k_2) were the same for $CheA^{wt}$ and $CheA^{F455W}$. Our measured K_{d} values (90 μM for $CheA^{F455W}$ and 350 μM for $CheA^{wt}$) indicate a ratio of 4.2, close to the expected value given the relative values of k_{-2}. This agreement supports the hypothesis that the active site of $CheA^{F455W}$ interacts with Mg−ATP in much the same way as does the wild-type active site, the only significant difference being the kinetics of the step that reverses the active site conformational change. This difference might reflect energetically favorable interaction of the W455 side chain with some nearby region of CheA in the "lid-closed" conformation.

In summary, these results support the conclusion that the fluorescence properties of $CheA^{F455W}$ can be used to monitor ATP-binding events and a conformational change at the CheA active site. This conformational change occurs rapidly relative to the rate of catalytic turnover and may reflect closure of the ATP lid region of the active site. In the future, W455 fluorescence might be useful for characterizing the effects of various mutations in or near the active site of CheA.

ACKNOWLEDGMENT

I thank Sandy Parkinson for *E. coli* strains and Ann Hirschman for plasmids. Ricaele VanBruggen helped create some of the *cheA* point mutants and to purify the corresponding proteins. Qinghua Cui performed initial characterization of some of the CheA variants.

REFERENCES

1. Hess, J. F., Oosawa, K., Matsumura, P., and Simon, M. I. (1987) Protein phosphorylation is involved in bacterial chemotaxis, *Proc. Natl. Acad. Sci. U.S.A. 84*, 7609−7613.
2. Hess, J. F., Bourret, R. B., and Simon, M. I. (1988) Histidine phosphorylation and phosphoryl group transfer in bacterial chemotaxis, *Nature 336*, 139−143.

3. Berg, H. C. (2004) *E. coli in motion*, Springer-Verlag, New York.
4. Eisenbach, M. (1996) Control of bacterial chemotaxis, *Mol. Microbiol. 20*, 903−910.
5. Stock, J., and Surette, M. G. (1996) in *Escherichia coli and Salmonella. Cellular and Molecular Biology* (Neidhardt, F. C., Ed.) pp 1103−1129, ASM Press, Washington, DC.
6. Borkovich, K. A., Kaplan, N., Hess, J. F., and Simon, M. I. (1989) Transmembrane signal transduction in bacterial chemotaxis involves ligand-dependent activation of phosphate group transfer, *Proc. Natl. Acad. Sci. U.S.A. 86*, 1208−1212.
7. Borkovich, K. A., and Simon, M. I. (1990) The dynamics of protein phosphorylation in bacterial chemotaxis, *Cell 63*, 1339−1348.
8. Ninfa, E. G., Stock, A. M., Mowbray, S., and Stock, J. (1991) Reconstitution of the bacterial chemotaxis signal transduction system from purified components, *J. Biol. Chem. 266*, 9764−9770.
9. Bourret, R. B., Borkovich, K. A., and Simon, M. I. (1991) Signal transduction pathways involving protein phosphorylation in prokaryotes, *Annu. Rev. Biochem. 60*, 401−441.
10. Hess, J. F., Oosawa, K., Kaplan, N., and Simon, M. I. (1988) Phosphorylation of three proteins in the signaling pathway of bacterial chemotaxis, *Cell 53*, 79−87.
11. Welch, M., Oosawa, K., Aizawa, S.-I., and Eisenbach, M. (1993) Phosphorylation-dependent binding of a signal molecule to the flagellar switch of bacteria, *Proc. Natl. Acad. Sci. U.S.A. 90*, 8787−8791.
12. Welch, M., Oosawa, K., Aizawa, S.-I., and Eisenbach, M. (1994) Effects of phosphorylation, Mg^{+2}, and conformation of the chemotaxis protein CheY on its binding to the flagellar switch protein FliM, *Biochemistry 33*, 10470−10476.
13. Lupas, A., and Stock, J. B. (1989) Phosphorylation of an N-terminal regulatory domain activates the methylesterase in bacterial chemotaxis, *J. Biol. Chem. 264*, 17337−17342.
14. Stewart, R. C., Roth, A. F., and Dahlquist, F. W. (1990) Mutations that affect control of the methylesterase activity of CheB, a component of the chemotaxis adaptation system in *Escherichia coli*, *J. Bacteriol. 172*, 3388−3399.
15. Hess, J. F., Bourret, R. B., Oosawa, K., Matsumura, P., and Simon, M. I. (1988) Protein phosphorylation and bacterial chemotaxis, *Cold Spring Harbor Symp. Quant. Biol. 53*, 41−48.
16. Parkinson, J. S., and Kofoid, E. C. (1992) Communication modules in bacterial signalling proteins, *Annu. Rev. Genet. 26*, 71−112.
17. Stock, A. M., Robinson, V. L., and Goudreau P. N. (2000) Two-component signal transduction, *Annu. Rev. Biochem. 69*, 183-215.
18. Mizuno, T. (1997) Compilation of all genes encoding two-component phosphotransfer signal transducers in the genome of *Escherichia coli*, *DNA Res. 4*, 161−168.
19. Grebe, T. W., and Stock, J. B. (1999) The histidine protein kinase superfamily, *Adv. Microb. Physiol. 41*, 139−227.
20. Pirrung, M. C. (1999) Histidine kinases and two-component signal transduction systems, *Chem. Biol. 6*, R167−R175.
21. Chang, C., and. Stewart, R. C. (1998) The two-component system: regulation of diverse signaling pathways in prokaryotes and eukaryotes, *Plant Physiol. 117*, 723−731.
22. Ellefson, D. D., Weber, U., and Wolfe, A. J. (1997) Genetic analysis of the catalytic domain of the chemotaxis-associated histidine kinase CheA, *J. Bacteriol. 179*, 825−830.
23. Hirschman, A., Boukhvalova, M., VanBruggen, R., Wolfe, A. J., and Stewart, R. C. (2001) Active site mutations in CheA, the signal-transducing protein kinase of the chemotaxis system in *Escherichia coli*, *Biochemistry 40*, 13876−13887.
24. Tawa, P., and. Stewart, R. C. (1994) Kinetics of CheA autophosphorylation and dephosphorylation reactions, *Biochemistry 33*, 7917−7924.
25. Wolfe, A. J., and Stewart, R. C. (1993) The short form of the CheA protein restores kinase activity an chemotactic ability to kinase-deficient mutants, *Proc. Natl. Acad. Sci. U.S.A. 90*, 1518−1522.
26. Swanson, R. V., Schuster, S. C., and Simon, M. I. (1993) Expression of CheA fragments which define domains encoding kinase, phosphotransfer, and CheY binding activities, *Biochemistry 32*, 7623−7629.
27. Levit, M., Liu, Y., Surette, M., and Stock, J. (1996) Active site interference and asymmetric activation in the chemotaxis protein histidine kinase CheA, *J. Biol. Chem. 271*, 32057−32063.
28. Surette, M. L., M., Liu, Y., Lukat, G., Ninfa, E., Ninfa, A., and Stock, J. (1996) Dimerization is required for the activity of the protein histidine kinase CheA that mediates signal transductin in bacterial chemotaxis, *J. Biol. Chem. 271*, 939−945.
29. Zhou, H., McEvoy, M. M., Lowry, D. F., Swanson, R. B., Simon, M. I., and Dahlquist, F. W. (1995) NMR studies of the phosphotransfer domain of the histidine kinase CheA from *Escherichia coli*: assignments, secondary structure, general fold, and backbone dynamics, *Biochemistry 34*, 13858−13870.
30. Zhou, H. J., McEvoy, M. M., Lowry, D. F., Swanson, R. V., Simon M. I., Dahlquist. F. W. (1996) Phosphotransfer and CheY-binding domains of the histidine autokinase CheA are joined by a flexible linker, *Biochemistry 35*, 433−443.
31. Bilwes, A., Alex., L., Crane, B. R., and Simon, M. I. (1999) Structure of CheA, a signal-transducing histidine kinase, *Cell 96*, 131−141.
32. Bilwes, A., Quezada, C. M., Croal, L. R., Crane, B. R., and Simon, M. I. (2001) Nucleotide binding by the histidine kinase CheA, *Nat. Struct. Biol. 8*, 353−360.
33. Marina, A., Mott, C., Auyzenberger, A., Hendrickson, W. A., and Waldburger, C. D. (2001) Structural and mutational analysis of the PhoQ histidine kinase catalytic domain, *J. Biol. Chem. 276*, 41182−41190.
34. Tanaka, T., Saha, S. K., Tomomori, C., Ishima, R., Liu, D., Tong, K. I., Park, H., Dutta, R., Qin, L, Swindells, M. B., Yamazaki, T., Ono, A. M., Kainosho, M., Inouye, M., and Ikura, M. (1998) NMR structure of the histidine kinase domain of the osmosensor EnvZ, *Nature 396*, 88−92.
35. Zhu, Y., and Inouye, M. (2002) The role of the G2 box, a conserved motif in the histidine kinase superfamily, in modulating the function of EnvZ, *Mol. Microbiol. 45*, 653−663.
36. Dutta, R., Qin, L., and Inouye, M. (1999) Histidine kinases: diversity of domain organization, *Mol. Microbiol. 34*, 633−640.
37. Wigley, D. B., Davies, G. J., Dodson, E. J., Maxwell, A., and Dodson, G. (1991) Crystal structure of an N-terminal fragment of the DNA gyrase B protein, *Nature 351*, 624−629.
38. Lewis, R. J., Singh, O. M., Smith, C. V., Skarzynski, T., Maxwell, A., Wonacott, A. J., and Wigley, D. B. (1996) The nature of inhibition of DNA gyrase by the coumarins and the cyclothialidines revealed by x-ray chrystallography, *EMBO J. 15*, 1412−1420.
39. Ban, C., and Yang, W. (1998) Crystal structure and ATPase activity of MutL: implications for DNA repair and mutagenesis, *Cell 95*, 541−552.
40. Dutta, R., and Inouye, M. (2000) GHKL, an emergent ATPase/kinase superfamily, *Trends Biochem. Sci. 25*, 24−28.
41. Stock, J. (1999) Signal transduction: gyrating protein kinases, *Curr. Biol. 9*, R364−R367.
42. Smith, R. A., and Parkinson, J. S. (1980) Overlapping genes at the *cheA* locus of *E. coli*, *Proc. Natl. Acad. Sci. U.S.A. 77*, 5370−5374.
43. Liu, J. (1990) Ph.D. Thesis, University of Utah, Salt Lake City, UT.
44. Wolfe, A. J., and Berg, H. C. (1989) Migration of bacteria in semisolid agar, *Proc. Natl. Acad. Sci. U.S.A. 86*, 6973−6977.
45. Smith, J. G., Latiolais, J. A., Guanga, G. P., Citineni, S., Silversmith, R. E., and Bourret, R. B. (2003) Investigation of the role of electrostatic charge in activation of the *Escherichia coli* response regulator CheY, *J. Bacteriol. 185*, 6385−6391.
46. Hess, J. F., Bourret, R. B., and Simon, M. I. (1991) Phosphorylation assays for proteins of the 2-component regulatory system controlling chemotaxis in *Escherichia coli*, *Methods Enzymol. 200*, 188−204.
47. Matsumura, P., Rydel, J. J., Linzmeier, R., and Vacante, D. (1984) Overexpression and sequence of the *Escherichia coli cheY* gene and biochemical activities of the CheY protein, *J. Bacteriol. 160*, 36−41.
48. Gill, S., and von Hippel, P. H. (1989) Calculation of protein extinction coefficients from amino acid sequence data, *Anal. Biochem. 182*, 319−326.
49. Norby, J. G. (1988) Coupled assay of Na^+, K^+-ATPase activity, *Methods Enzymol. 156*, 708−716.
50. Morrison, T. B., and Parkinson, J. S. (1994) Quantifying radiolabeled macromolecules and small molecules on a single gel, *Biotechniques 17*, 922−926.
51. Kuzmic, P. (1996) Program DYNAFIT for the analysis of enzyme kinetic data: application to HIV proteinase, *Anal. Biochem. 237*, 260−273.
52. Brissette, P., Ballou, D. P., and Massey, V. (1989) Determination of the dead time of a stopped-flow fluorometer, *Anal. Biochem. 181*, 234−238.
53. Hirschman, A. (2002) Ph.D. Thesis, University of Maryland, College Park, MD.

54. Stewart, R. C., VanBruggen, R., Ellefson, D. D., and Wolfe, A. J. (1998) TNP-ATP and TNP-ADP as probes of the nucleotide binding site of CheA, the histidine protein kinase in the chemotaxis signal transduction pathway of *Escherichia coli*, *Biochemistry 37*, 12269−12279.
55. Strickland, S., Palmer, G., and Massey, V. (1975) Determination of dissociation constants and specific rate constants of enzyme-substrate (or protein−ligand) interactions from rapid reaction kinetic data, *J. Biol. Chem. 250*, 4048−4052.
56. McEvoy, M. M., Zhou, J., Roth, A. F., Lowry, D. F., Morrison, T. B., Kay, L. E., and Dahlquist, F. W. (1995) Nuclear magnetic resonance assignments and global fold of a CheY-binding domain in CheA, the chemotaxis-specific kinase of *Escherichia coli*, *Biochemistry 34*, 13871−13880.
57. McEvoy, M. M., Muhandiram, D. R., Kay, L. E., and Dahlquist, F. W. (1996) Structure and dynamics of a CheY-binding domain of the chemotaxis kinase CheA determined by nuclear magnetic resonance spectroscopy, *Biochemistry 35*, 5633−5640.
58. McEvoy, M. M., Hausrath, A. C., Randolph, G. B., Remington, S. J., and Dahlquist, F. W. (1998) Two binding modes reveal flexibility in kinase/response regulator interactions in the bacterial chemotaxis pathway, *Proc. Natl. Acad. Sci. U.S.A. 95*, 7333−7338.
59. Welch, M. C., N., Mourey, L., Birck, C., and Samama, J.-P. (1997) Structure of the CheY-binding domain of histidine kinase CheA in complex with CheY, *Nat. Struct. Biol. 5*, 25−29.
60. Morrison, T. B., and Parkinson, J. S. (1994) Liberation of an interaction domain from the phosphotransfer region of CheA, a signaling kinase of *Escherichia coli*, *Proc. Natl. Acad. Sci. U.S.A. 91*, 5485−5489.
61. Morrison, T. B., and Parkinson, J. S. (1997) A fragment liberated from the E. coli kinase that blocks stimulatory, but not inhibitory, chemoreceptor signaling, *J. Bacteriol. 179*, 5543−5550.

BI0476026